Climatic Change
DOI 10.1007/s10584-013-0825-1

Assessing the influence of climate model uncertainty on EU-wide climate change impact indicators

Tobias Lung · Alessandro Dosio · William Becker · Carlo Lavalle · Laurens M. Bouwer

Received: 23 November 2012 / Accepted: 17 June 2013

Abstract Despite an increasing understanding of potential climate change impacts in Europe, the associated uncertainties remain a key challenge. In many impact studies, the assessment of uncertainties is underemphasised, or is not performed quantitatively. A key source of uncertainty is the variability of climate change projections across different regional climate models (RCMs) forced by different global circulation models (GCMs). This study builds upon an indicator-based NUTS-2 level assessment that quantified potential changes for three climate-related hazards: heat stress, river flood risk, and forest fire risk, based on five GCM/RCM combinations, and non-climatic factors. First, a sensitivity analysis is performed to determine the fractional contribution of each single input factor to the spatial variance of the hazard indicators, followed by an evaluation of uncertainties in terms of spread in hazard indicator values due to inter-model climate variability, with respect to (changes in) impacts for the period 2041–70. The results show that different GCM/RCM combinations lead to substantially varying impact indicators across all three hazards. Furthermore, a strong influence of inter-model variability on the spatial patterns of uncertainties is revealed. For instance, for river flood risk, uncertainties appear to be particularly

Electronic supplementary material The online version of this article (doi:10.1007/s10584-013-0825-1) contains supplementary material, which is available to authorized users.

T. Lung (✉) · A. Dosio · C. Lavalle
European Commission Joint Research Centre, Institute for Environment and Sustainability, Ispra, Italy
e-mail: tobias.lung@jrc.ec.europa.eu

T. Lung
e-mail: tobias.lung@eea.europa.eu

W. Becker
European Commission Joint Research Centre, Institute for the Protection and Security of the Citizen, Ispra, Italy

L. M. Bouwer
Deltares, Delft, The Netherlands

L. M. Bouwer
Institute for Environmental Studies, Vrije Universiteit, Amsterdam, The Netherlands

T. Lung
European Environment Agency, Copenhagen, Denmark

Published online: 05 July 2013

high in the Mediterranean, whereas model agreement is higher for central Europe. The findings allow for a hazard-specific identification of areas with low vs. high model agreement (and thus confidence of projected impacts) within Europe, which is of key importance for decision makers when prioritising adaptation options.

1 Introduction

Projected climatic changes in Europe over the coming decades are not limited to an increase in mean temperature but are expected to also affect other parameters such as precipitation patterns and weather extremes (IPCC 2007). There is strong agreement that these changes in climatic stimuli will have a substantial impact on natural and economic processes in Europe, and that potential impacts will vary in effect and magnitude, depending on region and sector (e.g. Alcamo et al. 2007). Much research has focussed on understanding the extent and spatial distribution of climate change impacts, with numerous, mostly sector-specific case studies as well as cross-sectoral efforts (e.g. EEA-JRC-WHO 2008) contributing to a gradually accumulating knowledge base. However, the assessment and communication of associated uncertainties remains a key challenge (Rosenzweig and Wilbanks 2010). Scepticism about the reliability of climate change impact assessment results, with underlying uncertainties in climate projections as one of the main factors, is repeatedly mentioned as obstacle for incorporating them into decision-making processes towards adaptation strategies (e.g. Rannow et al. 2010).

Uncertainties in impact assessment results are accumulated throughout the process of producing climate change projections and subsequent impact assessments as a cascading pyramid (Ahmad et al. 2001; Maslin and Austin 2012). The initial source of uncertainty in the causal chain relates to the assumptions on different pathways of anthropogenic greenhouse gas emissions and resulting atmospheric concentrations, followed by the ability of general circulation models (GCMs) to simulate changes in climatic parameters. Another layer of uncertainty is added by regional climate models (RCMs) forced by GCMs that are potentially able to better mimic local climate conditions, while bias correction, if applied, may cause some additional uncertainty (Hagemann et al. 2011). Uncertainty is further increasing when using climate projections as inputs to impact models that might combine the climate scenarios with non-climatic data, e.g. socio-economic factors, and projections of assets at risk.

Although uncertainties stemming from climate projections are mostly discussed qualitatively (e.g. Lissner et al. 2012; Rannow et al. 2010), the use of a single model projection is still practised (though decreasing) and uncertainties of climate projections are rarely assessed quantitatively. Also in approaches based on composite indicators (e.g. ESPON 2011), usually single climate simulations are used, rather than for instance the numerous high-resolution simulations for Europe provided by the projects PRUDENCE (Christensen et al. 2002) and ENSEMBLES (van der Linden and Mitchell 2009). Among impact studies that actually take account of climate uncertainty, a comparison among different SRES emission scenarios based on a single climate model is a widespread approach, e.g. Carvalho et al. (2010). A number of studies consider multiple realisations of the same GCM but with varying parameters (perturbed physics ensemble, PPE), e.g. Lopez et al. (2009). Some impact studies so far have taken into account multiple GCM/RCM combinations, using data from the PRUDENCE project, e.g. assessments related to floods (Dankers and Feyen 2009) or sea level rise (Hinkel et al. 2010), or employing several ENSEMBLES GCM/RCM combinations, e.g. for studying hydrological changes/floods (Olsson et al. 2011; Rojas et al. 2012) or wind storms (Donat et al. 2011). However, even where impact studies have used multiple models, it is debatable to what extent uncertainty has been addressed systematically.

With the present study we aim at studying the influence of uncertainties in the projected climate amongst high resolution RCM simulations from the ENSEMBLES project on an indicator-based impact assessment for three climate-related hazards (Lung et al. 2013). The results of this pan-European regional level assessment are now evaluated in detail in terms of changes due to the choice of ENSEMBLES GCM/RCM combination, the emission scenario being invariant, i.e. SRES-A1B. The paper first presents a sensitivity analysis of the composite indicators of Lung et al. (2013), that are based on the average of five ENSEMBLE simulations, determining the fractional contribution of each single climatic and non-climatic input indicator. Secondly, for each of the three composite indicators, calculations with data from individual ENSEMBLE simulations are studied and the patterns of composite indicator agreement/spread across Europe are evaluated.

2 Material and methods

2.1 Hazard-specific impact indicators at NUTS-2 level

The basis for this paper is the study by Lung et al. (2013), referred to as L13 in the following, that presents an indicator-based impact assessment at NUTS-2 regional level. L13 quantify potential regional changes for three climate-related hazards: heat stress in relation to human health, river flood risk, and forest fire risk. Following a framework proposed by Füssel and Klein (2006), single-input indicators representing climate exposure and sensitivity were combined to hazard-specific composite indicators. The L13 analysis comprises a baseline situation, with climate data from 1961 to 1990, a short-term scenario 2011–2040, and a medium-term scenario 2041–2070. For each hazard, climate indicators calculated from ENSEMBLES data were employed to represent exposure. Non-climatic drivers (e.g. socio-economic change, land use) were used to represent sensitivity (defined in L13 as the dose–response relationship between climate exposure and the resulting impacts). Five ENSEMBLES experiments were selected from the various combinations of RCMs and GCMs (for details see Section 2.2), and for each single climate indicator the mean across these five experiments was used for the final hazard indicators of L13.

During composite indicator construction, all input indicators were transformed into dimensionless z-scores centred on zero (i.e. with a mean of zero and a standard deviation of one), using the baseline EU mean and standard deviation. For combining them into composite hazard indicators, geometric aggregation (i.e. the product of weighted indicators) was employed, giving equal weight to the single indicators. Each final hazard indicator was classified into five impact categories (‘very low’, ‘low’, ‘medium’, ‘high’, ‘very high’) according to percentile thresholds (i.e. 0–20 %, 20–40 %, etc.). The categories represent relative impacts between European regions. For the scenario periods the percentile thresholds of each baseline composite indicator were applied. In addition, percentage changes of each composite hazard indicator from baseline to 2041–2070 were calculated.

While for heat stress only temperature-related climate input indicators were used, the forest fire risk indicator employs indicators of both temperature and precipitation (Table 1). For constructing the flood risk indicator, climate indicators were fed into the flood simulation model LISFLOOD (van der Knijff et al. 2010), whose outputs (i.e. inundation extent and water depth) were then used for building the composite indicator. It is important to note that due to this additional step of hydrological modelling, the flood risk indicator is somewhat different from the other two indicators: results are not only determined by climate information, but also by assumptions about the hydrological response of river catchments, river flow routing and inundation extents. The response of the flood hazard to precipitation

Table 1 First-order sensitivity indices of input indicators for the three composite indicators of Lung et al. (2013): **a** heat stress, **b** river flood risk, and (**c**) forest fire risk

Indicator type	(a) Heat stress		(b) River flood risk		(c) Forest fire risk	
	Name	S_i	Name	S_i	Name	S_i
Climatic	TCOMB[a]	0.400	AREA[d]	0.237	CDDMAX[h]	0.206
			DPTH[e]	0.277	T2MEANsu[i]	0.153
					PRECsu[j]	0.156
Non-climatic	POPD[b]	0.322	POPD[f]	0.241	WILDL[k]	0.184
	PCOMB[c]	0.282	COM[g]	0.251	ACCESS[l]	0.160
					COMBU[m]	0.161

[a] Mean of T2MAX25 (Number of summer days with T_{max}>25 °C in summer period [JJA]) and T2MIN20 (Number of tropical nights with T_{min}>20 °C in summer period [JJA])

[b] Population density [in people/km^2]

[c] Mean of POP75 (percentage of elderly people>75 years) and HH65 (Percentage of households composed of one adult>65 years)

[d] Percentage of flooded area, magnitude of a 100-year event flood

[e] Mean water depth [in m] of flooded area, magnitude of a 100-year event flood

[f] Population density within areas affected by 100-year recurrence interval flood

[g] Percentage of commercial & industrial areas affected by 100-year recurrence interval flood

[h] Greatest number of consecutive days per year with daily precipitation<1 mm

[i] Mean of daily mean summer temperature [JJA]

[j] Summer precipitation [JJA]

[k] Percentage of wildland [CLC classes 311, 312, 313, 321, 323, 324]

[l] Mean fuel type combustibility

[m] Wildland accessibility by roads

changes is non-linear in nature, thus leading locally to potentially larger variations in flood occurrence compared to other precipitation related hazards such as forest fire risk. In addition, the flood risk indicator represents only (changes in) the frequency of high-discharge events with 100-year recurrence intervals (Feyen et al. 2012; Lung et al. 2013).

2.2 ENSEMBLES climate model projections

Climatic data from the ENSEMBLES project was corrected for biases in temperature and precipitation (Dosio and Paruolo 2011; Dosio et al. 2012), who applied a statistical technique developed by Piani et al. (2010). Even though adding another level of uncertainty, several studies have shown that bias-corrected climate data may lead to improved impact assessment results (e.g. Teutschbein and Seifert 2010). As process-based impact models are often too expensive on time and resources to be run using a large ensemble of climate runs, Dosio et al. (2012) suggested to use a subset that represents both the main statistical properties of the whole ensemble (i.e. the climate change signal), and the most extreme deviations from it, i.e. those that maximise the variability. In L13, five ENSEMBLE runs were selected (Table 2), aiming at maximising the number of GCM/RCM combinations. This selection is somewhat subjective, and other criteria may lead to different subsets. All the models are driven by the same emission scenario (SRES-A1B) and thus, all runs represent an equally probable projection of the future evolution of the climate. As inter-model

Table 2 Climate input indicators[a] of the heat stress and forest fire risk composite indicators, as well as flood hazard input for river flood risk composite indicator; given as ensemble means and their model-specific[b] mean deviations, per impact category by Lung et al. (2013) for 2041–2070. For each input indicator, the maximum and minimum model-specific deviation is highlighted in bold

	EIR, scenario 2041–2070				
	very low	low	medium	high	very high
Heat stress					
T2MAX25, ENSEMBLE MEAN [no. of days]	*11.80*	*26.51*	*30.77*	*44.70*	*47.23*
T2MAX25, C4I-RCA-HadCM3Q16	**3.78**	**6.16**	**5.33**	**3.74**	**4.35**
T2MAX25, CNRM-ALADIN-ARPEGE	−0.06	2.37	2.51	3.00	3.32
T2MAX25, DMI-HIRHAM-ECHAM5	**−2.94**	**−7.17**	**−6.79**	**−6.13**	**−7.13**
T2MAX25, ETHZ-CLM-HadCM3Q0	2.28	3.69	3.53	3.15	3.93
T2MAX25, SMHI-RCA-BCM	−2.90	−4.92	−4.57	−3.76	−4.46
T2MIN20, ENSEMBLE MEAN [no. of days]	*0.58*	*1.69*	*3.24*	*10.73*	*12.12*
T2MIN20, C4I-RCA-HadCM3Q16	**0.89**	**2.33**	**2.86**	**4.77**	**5.78**
T2MIN20, CNRM-ALADIN-ARPEGE	0.21	0.79	1.05	2.76	3.15
T2MIN20, DMI-HIRHAM-ECHAM5	**−0.42**	**−1.46**	**−1.95**	**−4.06**	**−4.80**
T2MIN20, ETHZ-CLM-HadCM3Q0	−0.32	−0.93	−1.06	−1.66	−1.72
T2MIN20, SMHI-RCA-BCM	−0.37	−0.74	−0.90	−1.82	−2.42
Forest fire risk					
CDDMAX, ENSEMBLE MEAN [no. of days]	*19.83*	*21.18*	*23.10*	*23.96*	*59.72*
CDDMAX, C4I-RCA-HadCM3Q16	−1.41	−1.58	−1.14	−1.20	0.39
CDDMAX, CNRM-ALADIN-ARPEGE	**3.91**	**5.31**	**3.77**	4.90	−3.98
CDDMAX, DMI-HIRHAM-ECHAM5	**−2.66**	**−3.90**	**−3.05**	**−4.51**	−1.33
CDDMAX, ETHZ-CLM-HadCM3Q0	2.23	3.20	3.18	**4.91**	**15.80**
CDDMAX, SMHI-RCA-BCM	−2.08	−3.03	−2.76	−4.10	**−10.89**
T2MEANsu, ENSEMBLE MEAN [in °C]	*15.57*	*17.28*	*18.29*	*19.09*	*23.46*
T2MEANsu, C4I-RCA-HadCM3Q16	**1.02**	**0.91**	**1.10**	**0.91**	**1.27**
T2MEANsu, CNRM-ALADIN-ARPEGE	−0.02	0.12	0.19	0.44	0.39
T2MEANsu, DMI-HIRHAM-ECHAM5	−0.62	**−0.81**	**−1.26**	**−1.29**	**−1.12**
T2MEANsu, ETHZ-CLM-HadCM3Q0	0.29	0.35	0.43	0.50	−0.04
T2MEANsu, SMHI-RCA-BCM	**−0.67**	−0.58	−0.47	−0.56	−0.50
PRECsu, ENSEMBLE MEAN [in mm]	*226.76*	*184.69*	*205.17*	*176.12*	*66.14*
PRECsu, C4I-RCA-HadCM3Q16	−22.85	−16.86	−20.56	−23.90	−9.87
PRECsu, CNRM-ALADIN-ARPEGE	1.59	−12.38	2.81	−7.69	7.69
PRECsu, DMI-HIRHAM-ECHAM5	**39.53**	**39.00**	**39.29**	**41.04**	8.55
PRECsu, ETHZ-CLM-HadCM3Q0	**−38.82**	**−34.20**	**−46.21**	**−42.63**	**−25.90**
PRECsu, SMHI-RCA-BCM	20.55	24.44	24.67	33.18	**19.53**
River flood risk					
AREA[c], ENSEMBLE MEAN [% of NUTS-2]	*0.976*	*2.713*	*2.838*	*4.902*	*9.192*
AREA, C4I-RCA-HadCM3Q16	−0.150	−0.331	−0.274	−0.547	**−0.572**
AREA, CNRM-ALADIN-ARPEGE	−0.150	−0.404	−0.448	−0.805	−1.015
AREA, DMI-HIRHAM-ECHAM5	−0.173	−0.411	−0.542	−0.909	−1.085
AREA, ETHZ-CLM-HadCM3Q0	**−0.027**	**−0.186**	**−0.171**	**−0.324**	−0.591
AREA, SMHI-RCA-BCM	**−0.175**	**−0.487**	**−0.621**	**−1.037**	**−1.354**
DPTH[d], ENSEMBLE MEAN [in m]	*1.085*	*1.379*	*1.633*	*1.652*	*1.899*

Table 2 (continued)

	EIR, scenario 2041–2070				
	very low	low	medium	high	very high
DPTH, C4I-RCA-HadCM3Q16	0.131	0.220	0.368	0.304	0.285
DPTH, CNRM-ALADIN-ARPEGE	0.087	0.185	0.202	0.212	0.171
DPTH, DMI-HIRHAM-ECHAM5	0.083	0.127	0.124	0.193	0.191
DPTH, ETHZ-CLM-HadCM3Q0	**0.384**	**0.344**	**0.450**	**0.411**	**0.350**
DPTH, SMHI-RCA-BCM	**0.044**	**0.081**	**0.082**	**0.107**	**0.064**

[a] see Table 1 for indicator names and descriptions

[b] for a full description of the institutes' acronyms, the RCMs and GCMs, see Christensen et al. (2010)

[c] Flood extent (AREA) in L13 was based on binary values (i.e. no inundation if none of the five ENSEMBLES models simulates inundation, or inundation if one or more models indicate inundation). Therefore, for each NUTS-2 region the ensembles flood extent shows the largest value, and for the individual ENSEMBLES model projections only negative deviations from that ensemble extent are seen.

[d] Water depth (DPTH) in L13 was averaged over the five water depth projections, including those models that simulate no inundation (i.e. zero values). Therefore, only positive deviations from the ensemble are revealed.

climate variability increases over time (Dosio et al. 2012), this study focuses on analysing only the latest scenario of L13, i.e. the medium-term scenario 2041–70.

2.3 Sensitivity analysis of impact indicators

Prior to analysing the impact of climate model variability on composite hazard indicators, the fractional contribution of each climatic and non-climatic input indicator to the spatial variance of the composite indicators of L13 was examined. A global variance-based approach was adopted that examines the simultaneous variation of all inputs to a system, as opposed to varying one input at a time (Saltelli et al. 2008).

Variance-based sensitivity analysis expresses the sensitivity of the output Y of the composite indicator to each of its d inputs $\{X_i\}_{i=1}^{d}$ as the fraction of output variance caused by each input or combination of inputs (Sobol' 1993). In this work the *total effect index* is used, which is given as,

$$S_{Ti} = \frac{E_{X_{\sim i}}\left(\mathrm{var}_{X_i}\left(Y \middle| X_{\sim i}\right)\right)}{\mathrm{var}(Y)}$$

Where $E_{X_{\sim i}}$ denotes the expected value over all inputs except the ith. This measures the contribution to the variance of the indicator by the input i, and its interactions with all other inputs (Jansen 1999). An alternative approach would be to use the *first order sensitivity index* (Sobol' 1993) which does not measure the effects of interactions. Although the construction of the L13 indicators prohibits interactions, the total effect index is still used since this would be the prudent approach in the usual case where interactions cannot be discounted; in any case, it is by definition equal to the first order index when no interactions are present. For a full discussion on variance-based sensitivity analyses see Saltelli et al. (2008).

S_{Ti} can be estimated by the Monte Carlo method, which involves evaluating the indicator a large number of times at different input values specified by a Monte Carlo estimator (Saltelli et al. 2010). Monte Carlo sampling was performed with respect to the probability distributions of

the X_i. Here, there were 261 samples (one per NUTS-2) to define each input distribution. Some of the distributions are skewed or bimodal, which precludes the possibility of fitting standard analytical distributions. To obtain the best estimate of the underlying distribution, a kernel density estimation procedure (Botev et al. 2010) was used which smoothes the histograms into continuous distributions, allowing Monte Carlo samples to be drawn with respect to a continuous distribution (see Fig. 1 for an illustration).

Note that this approach requires an assumption of independence between inputs, despite the presence of correlation in the data here (up to 0.88, but generally below 0.3). Although this taints the outcome somewhat, the results are still indicative of the division of variance. In addition to the pan-European analysis, the procedure of deriving S_{Ti} was repeated dividing Europe into 5 macro-regions, in order to understand the uncertainty due to spatial resolution.

2.4 Assessing the influence of climate model variability on impact indicators

The influence of climate model variability was assessed based on calculations of the three hazard-specific impact indicators using the input indicators from each of the five individual climate models. The remainder of the paper uses the term '*individual model impact result*' (IMIR) to denote a composite impact indicator calculated with climate data from one of the five individual climate experiments, while the composite impact indicators based on the mean of all five climate models as mapped in L13 are referred to as '*ensemble impact result*' (EIR). All non-climatic sensitivity parameters were kept constant. As a first measure of indicator spread due to climate model variability, rank differences across the 261 NUTS-2 regions were calculated, subtracting the EIR ranks (i.e. 1 for the region with the highest, 261 for the region with the lowest indicator value) from the IMIR ranks for each of the five models and each of the three hazards. Furthermore, mean IMIR deviation from EIR was calculated in relation to (a) the extent of projected hazard impact in 2041–2070, and (b) the magnitude of projected EIR impact change. While (a) was assessed based on impact category (very high, high, medium, low, and very low), (b) was calculated using the categories of percentage change as presented in L13 (i.e. ≤0, 0–1, 1–2, 2–3, 3–4, >4). In addition, as a measure of within NUTS-2 indicator spread, the range between the minimum and the maximum IMIR value is presented as a map, in order to evaluate spatial patterns within Europe.

As an alternative way of assessing indicator spread in relation to the magnitude of projected change, indicator agreement was calculated, defined iteratively as the number of IMIRs falling within the absolute bounds of +/−1 % compared to the EIR change. For instance, if the change of an EIR in a NUTS-2 region was +3.4 %, the bounds would be 2.4 % and 4.4 %. Assuming IMIR changes of e.g. +2.9, +3.1, +1.5, +4.0, and +3.8, would lead to a model agreement of '4 out of 5' (i.e. only +1.5 would be outside the bounds). This

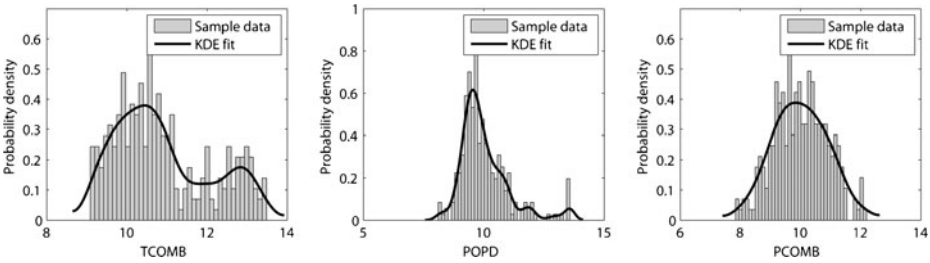

Fig. 1 Kernel density estimates of distributions of inputs to the heat stress indicator of Lung et al. (2013) (for indicator names see Table 1)

approach is preferable over relative bounds defined as percentage of percentage change, as these would introduce very narrow bounds (and thus misleadingly low agreement) for regions with low EIR change (e.g. bounds of +/−20 % for an EIR of 1 % would lead to bounds of 0.8 % and 1.2 %, instead of 0 % and 2 % when using absolute bounds). The results of the indicator agreement calculation are mapped as well.

3 Results

3.1 Sensitivity of hazard-specific impact indicators

Table 1 shows the S_{Ti} values of each indicator to its inputs. The results show that the contribution of each input is, in general, evenly divided for all three composite indicators. Since the composite indicators have fairly evenly-weighted input indicators, the sensitivity indices here reflect the different variances of the inputs. The kernel density estimation of the histograms was however necessary to investigate any possible effect of the shapes of the input distributions. Even though the sensitivity indices are somewhat similar, it is revealed that TCOMB has a strong impact on driving the heat stress indicator, and that CDDMAX is a stronger driver of the fire indicator than the two other climate input indicators (PRECsu and T2MEANsu). All three composite indicators of L13 are affected by each of their respective climatic as well as non-climatic input indicators to a significant degree.

3.2 Impact indicator spread due to climate input data

Rank differences for the three hazards generally indicate the largest IMIR spread for river flood risk, a medium spread for heat stress, and the smallest spread for forest fire risk (Fig. 2a). While for forest fire risk 79 % of IMIR ranks shift in the range [+/−10], this rate is 72 % for the heat stress IMIR ranks and 65 % for the flood risk IMIR ranks. For heat stress, in particular the DMI-HIRHAM-ECHAM5-based IMIR shows a larger spread (i.e. a higher number of rank differences larger than +/−15 and a less pronounced peak, see green graph in Fig. 2a) compared to the other IMIRs. A similar spread that is larger than the other models can also be seen for river flood risk for the ETHZ-CLM-HadCM3Q0-based IMIR.

3.2.1 Spread in relation to EIR impact categories

For heat stress, the DMI-HIRHAM-ECHAM5-based IMIR reveals considerably larger mean deviations (and thus spread) from EIR impact than the other IMIRs (Fig. 2b). This is due to a considerably lower number of both summer days (T2MAX25) and tropical nights (T2MIN20) projected by the DMI-HIRHAM-ECHAM5 model than the ensemble average (Table 2). The ETHZ-CLM-HadCM3Q0-based IMIR shows the lowest deviations of all IMIRs across all heat stress impact categories, due to a compensating effect between above-average values for T2MAX25 and below-average values for T2MIN20 (Table 2). For river flood risk, the ETHZ-CLM-HadCM3Q0-based IMIR shows the largest deviations across all EIR impact categories (Fig. 2b). This is due to the largest flood extent (obvious from the smallest deviation for this model from the ensemble mean flood extent; Table 2), and the largest water depth (largest deviations for this model from the ensemble mean water depth; Table 2) projected by the ETHZ-CLM-HadCM3Q0 model. For forest fire risk, again the DMI-HIRHAM-ECHAM5-based IMIR reveals the largest deviations (Fig. 2b), due to a

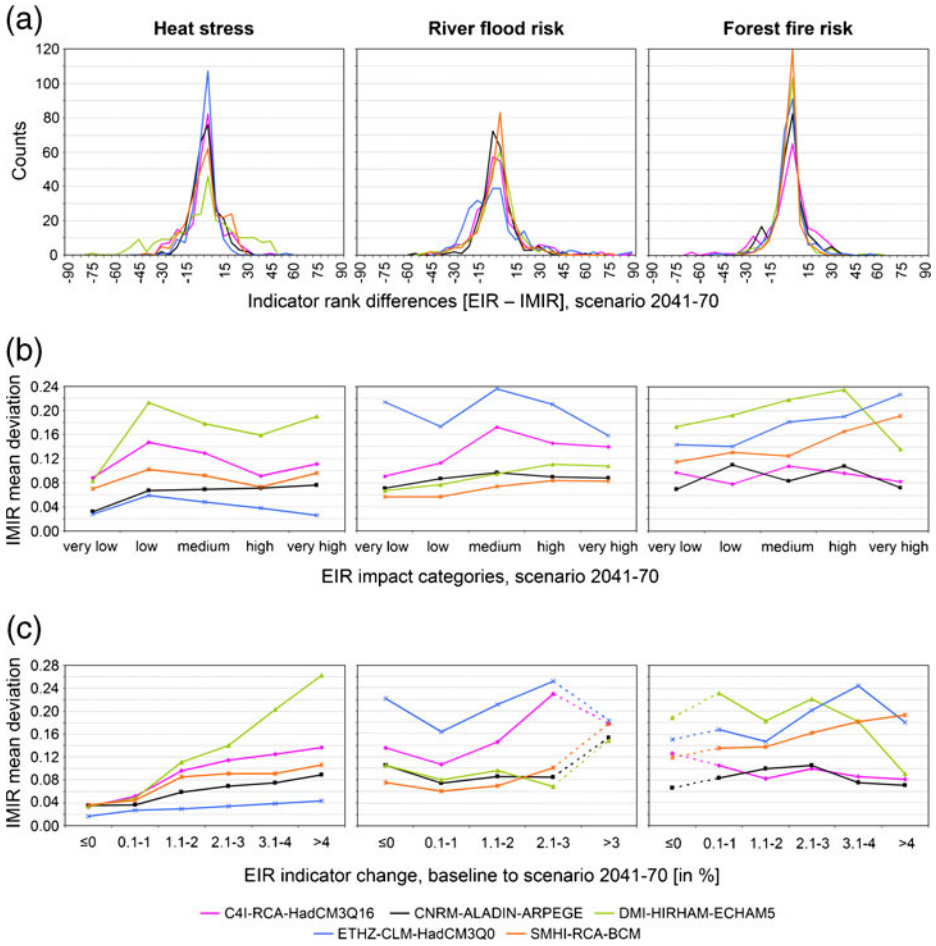

Fig. 2 Results from assessing the influence of climate model variability on composite indicators of heat stress, river flood risk, and forest fire risk of Lung et al. (2013) for the period 2041–2070, with respect to (**a**) rank differences between individual model impact results (IMIRs) and ensemble impact results (EIRs), **b** mean absolute deviation of IMIRs from EIRs per EIR category, and (**c**) mean absolute deviation of IMIRs from EIR per EIR change category. Dashed lines indicate that the respective category of change contains less than 5 % of all 261 NUTS-2 regions, and thus its results should be interpreted with caution

combination of factors least favourable for forest fires, namely few dry days (CDDMAX), the lowest mean summer temperature (T2MEANsu), and highest summer precipitation (PRECsu) (Table 2). For the very high impact regions, the DMI-HIRHAM-ECHAM5 model shows values closer to ensemble average for CDDMAX and PRECsu (Table 2), and consequently the DMI-HIRHAM-ECHAM5-based IMIR drops sharply (Fig. 2b).

3.2.2 Spread in relation to EIR change

Regarding the magnitude of projected EIR change in heat stress from the baseline to 2041–2070, an increase of IMIR deviation with increasing EIR change is seen for all five climate models, while the DMI-HIRHAM-ECHAM5-based IMIR shows strong mean deviations in

Table 3 Climate input indicators of the heat stress and forest fire risk composite indicators, as well as flood hazard input for river flood risk composite indicator; given as ensemble means and their model-specific mean deviations, per impact change category (from baseline to scenario 2041–2070) by Lung et al. (2013). For each input indicator, the maximum and minimum model-specific deviation is highlighted in bold

	EIR, change from baseline to scenario 2041–2070					
	< 0	0–1	1–2	2–3	3–4	>4
Heat stress						
T2MAX25, ENS. MEAN [no. of days]	*34.25*	*33.11*	*29.36*	*40.74*	*46.23*	*45.53*
T2MAX25, C4I-RCA-HadCM3Q16	1.59	1.68	**3.99**	**4.92**	**5.10**	**5.87**
T2MAX25, CNRM-ALADIN-ARPEGE	**2.21**	**1.89**	2.60	2.17	3.24	3.50
T2MAX25, DMI-HIRHAM-ECHAM5	**−2.38**	**−2.77**	**−5.37**	**−6.29**	**−7.86**	**−8.96**
T2MAX25, ETHZ-CLM-HadCM3Q0	1.63	2.27	3.45	3.35	4.08	4.61
T2MAX25, SMHI-RCA-BCM	−3.05	−3.07	−4.57	−4.11	−4.56	−4.99
T2MIN20, ENS. MEAN [no. of days]	*17.67*	*10.86*	*7.40*	*11.03*	*8.85*	*7.09*
T2MIN20, C4I-RCA-HadCM3Q16	**4.43**	**3.44**	**2.60**	**5.12**	**6.10**	**5.11**
T2MIN20, CNRM-ALADIN-ARPEGE	3.55	2.46	1.53	2.60	2.69	2.40
T2MIN20, DMI-HIRHAM-ECHAM5	**−3.89**	**−2.64**	**−1.95**	**−4.21**	**−4.65**	**−4.24**
T2MIN20, ETHZ-CLM-HadCM3Q0	−1.69	−1.51	−0.76	−1.48	−1.93	−1.44
T2MIN20, SMHI-RCA-BCM	−2.39	−1.75	−1.42	−2.02	−2.21	−1.84
Forest fire risk						
CDDMAX, ENS. MEAN [no. of days]	*21.30*	*22.84*	*22.01*	*27.57*	*50.98*	*69.54*
CDDMAX, C4I-RCA-HadCM3Q16	−1.55	−1.62	−1.42	−0.36	−1.09	2.12
CDDMAX, CNRM-ALADIN-ARPEGE	**3.90**	**4.56**	**4.79**	2.96	−0.45	−8.41
CDDMAX, DMI-HIRHAM-ECHAM5	−2.38	−3.44	**−3.67**	−3.62	−4.36	4.97
CDDMAX, ETHZ-CLM-HadCM3Q0	2.82	3.96	3.54	**5.39**	**14.72**	**14.70**
CDDMAX, SMHI-RCA-BCM	**−2.80**	**−3.46**	−3.24	**−4.38**	**−8.82**	**−13.38**
T2MEANsu, ENS. MEAN [in °C]	*18.04*	*18.99*	*17.54*	*18.90*	*22.28*	*23.84*
T2MEANsu, C4I-RCA-HadCM3Q16	**1.10**	**0.98**	**0.93**	**0.99**	**1.17**	**1.51**
T2MEANsu, CNRM-ALADIN-ARPEGE	0.14	0.47	0.09	0.37	0.34	0.62
T2MEANsu, DMI-HIRHAM-ECHAM5	**−1.19**	**−1.40**	**−0.83**	**−1.16**	**−1.11**	**−1.32**
T2MEANsu, ETHZ-CLM-HadCM3Q0	0.38	0.40	0.39	0.40	0.16	−0.40
T2MEANsu, SMHI-RCA-BCM	−0.43	−0.45	−0.57	−0.60	−0.56	−0.41
PRECsu, ENS. MEAN [in mm]	*199.57*	*184.59*	*179.51*	*188.89*	*92.47*	*58.84*
PRECsu, C4I-RCA-HadCM3Q16	−34.11	−28.73	−16.54	−22.49	−12.82	−6.71
PRECsu, CNRM-ALADIN-ARPEGE	13.07	−0.66	−10.65	−1.64	4.85	11.82
PRECsu, DMI-HIRHAM-ECHAM5	**36.20**	**42.62**	**36.09**	**39.00**	18.71	−0.83
PRECsu, ETHZ-CLM-HadCM3Q0	**−39.77**	**−40.45**	**−34.71**	**−45.05**	**−31.78**	**−20.61**
PRECsu, SMHI-RCA-BCM	24.61	27.22	25.81	30.18	**21.04**	**16.33**
River flood risk						
AREA, ENSEMBLE MEAN [% of NUTS-2]	*4.578*	*4.204*	*3.808*	*7.606*	*2.887*[a]	
AREA, C4I-RCA-HadCM3Q16	−0.493	−0.324	−0.405	−0.430	−0.204[a]	
AREA, CNRM-ALADIN-ARPEGE	**−0.486**	−0.530	−0.634	−1.531	−0.175[a]	
AREA, DMI-HIRHAM-ECHAM5	−0.657	−0.458	−0.678	−2.096	−0.236[a]	
AREA, ETHZ-CLM-HadCM3Q0	−0.512	**−0.161**	**−0.206**	**−0.369**	**−0.172**[a]	
AREA, SMHI-RCA-BCM	**−0.733**	**−0.565**	**−0.850**	**−2.289**	**−0.307**[a]	
DPTH, ENSEMBLE MEAN [in m]	*1.523*	*1.523*	*1.520*	*1.690*	*2.178*[a]	

Table 3 (continued)

	EIR, change from baseline to scenario 2041–2070					
	< 0	0–1	1–2	2–3	3–4	>4
DPTH, C4I-RCA-HadCM3Q16	0.229	0.223	0.298	0.430	0.549[a]	
DPTH, CNRM-ALADIN-ARPEGE	0.197	0.148	0.186	0.172	0.218[a]	
DPTH, DMI-HIRHAM-ECHAM5	0.182	0.119	0.166	0.151	0.071[a]	
DPTH, ETHZ-CLM-HadCM3Q0	**0.446**	**0.303**	**0.380**	**0.607**	**0.668**[a]	
DPTH, SMHI-RCA-BCM	**0.098**	**0.076**	**0.070**	**0.095**	**0.025**[a]	

[a] Due to very few occurrences, the impact change categories 3–4 and >4 have been grouped to a single category >3

particular for regions with an EIR increase greater than 3 (Fig. 2c). This is due to the fact that DMI-HIRHAM-ECHAM5 is an exceptionally cold model, in particular in regions where heat stress is projected to increase the most (Table 3). For river flood risk, the lowest deviations for most IMIRs are revealed for regions with only slight EIR increases (i.e. between 0.1 and 1), while strongest deviations that are sharply increasing with EIR change are seen for the ETHZ-CLM-HadCM3Q0 and C4I-RCA-HadCM3Q16-based IMIRs (Fig. 2c). These two models project significantly larger changes in flood extent and water depth (cf. previous paragraph). For fire risk, strong mean deviations are seen for the DMI-HIRHAM-ECHAM5 and ETHZ-CLM-HadCM3Q0-based IMIRs that drop sharply for regions where EIR impact is projected to increase the most (i.e. >4, Fig. 2c). For DMI-HIRHAM-ECHAM5, this pattern is linked to cold (below T2MEANsu average) and wet (below CDDMAX average and above PRECsu average) values except for regions with strong EIR increase, for which much drier values for CDDMAX and PRECsu are revealed (Table 3), thus causing the IMIR drop seen in Fig. 2c. The ETHZ-CLM-HadCM3Q0 pattern is explained by the contrary, i.e. very favourable forest fire conditions with values strongly above average CDDMAX, strongly below average PRECsu, and slightly above average T2MEANsu (Table 3).

3.2.3 Spatial patterns across Europe

The spatial pattern of IMIR heat stress range across European regions shows highest values for central and north-eastern Europe, as well as in southern Scandinavia (red and dark purple areas in Fig. 3a). These areas coincide to a large extent with those regions that show the highest rates of projected EIR heat stress increases (blue hatching in Fig. 3a), which is true for southern Germany in particular. In contrast, the southernmost regions of Portugal, Spain, Italy and Greece mostly show small IMIR ranges. Likewise, the analysis of model agreement reveals 'hotspot' regions of disagreement in southern Sweden and central Europe, in particular southern Germany, and mostly strong agreement for the UK and southern Europe (Fig. 3a).

For river flood risk, compared to the two other hazards, a patchy and spatially more inhomogeneous pattern of IMIR range is seen, very similar to the previous work in L13 (Fig. 3b). The majority of regions with high values are found in southern Europe, in particular along the coast of Spain, in (northern) Italy, Greece and the Danube delta (Fig. 3b). In addition, clusters of regions with high IMIR ranges are revealed in western Germany, Belgium and the Netherlands, as well as in Poland, the latter cluster being more clearly seen from the analysis in terms

Fig. 3 Maps of *i*) range (minimum – maximum) of five individual model impact results (IMIRs), and *ii*) IMIR agreement, displayed together with the magnitude of EIR change from baseline to 2041–70 (in percentage), for (**a**) heat stress, **b** river flood risk, and (**c**) forest fire risk. Note that regions showing no EIR change or an EIR decrease are displayed without any hatching

of model agreement (right map in Fig. 3b). No apparent linkage is revealed between regions of high IMIR range or model agreement and projections of strong EIR increases in flood risk.

Regarding forest fire risk, highest IMIR ranges are revealed for an area stretching from northern Spain into southern Germany and the Alpine region, thereby covering most parts of France (Fig. 3c). A similar but slightly northwards shifted pattern is revealed in terms of model agreement, showing strongest model disagreement in northern France and large parts of Germany as well as for a cluster of regions in south-eastern Poland/eastern Slovakia/eastern Hungary (Fig. 3c). In contrast, regions with highest rates of projected EIR fire risk increases in southern Spain, Italy, and Greece reveal medium or low IMIR ranges and high levels of model agreement (i.e. mostly 4 or 5 of 5, Fig. 3c). Similar results with low ranges and high agreement for revealed for the UK, Scandinavia, and the Baltic States.

4 Discussion and conclusions

The sensitivity analysis results have shown that the climate input indicators account for around 40 % (heat stress) or 50 % (river flood risk, forest fire risk) of the composite indicator variations at the pan-European level, therefore underpinning their importance in driving the composite indicators and reinforcing the necessity of assessing the impact of inter-model variability on the composite indicators. The macro-regional level analysis (for details see Supplementary material) demonstrated that spatial variations (and thus importance of indicator inputs) may vary, therefore calling for more in-depth local analysis of certain parameters in certain regions to avoid maladaptation. For example, in Scandinavia, water depth and commercial/industrial areas appear to play a particular crucial role in driving regional differences in flood risk.

It was shown that climate data from different models (here GCM/RCM combinations) may lead to substantially varying indicator-based impact assessment results. For each hazard-specific assessment, particular climate models appear to deviate considerably from the ensemble mean, which in turn resulted in impact results strongly differing from the ensemble mean. Moreover, these differences may vary greatly according to the degree of projected impact and/or the magnitude of projected impact change. For indicator-based approaches this clearly calls for the use of as many climate simulations as possible, in order to derive maximally robust impact results (cf. Rojas et al. 2012), or alternatively, to conduct a targeted model pre-selection driven by study purpose. Furthermore, it calls for a careful evaluation and use of indicator-based results by decision makers.

Climate model spread may have a large influence on the spatial patterns of uncertainties across Europe found in impact indicators, as already indicated in L13. This detailed study revealed that some trends of hazard change shown in L13 might be associated with a higher degree of uncertainty due to climate model spread than others. Also, it is noteworthy that some of these patterns are somewhat different to what would be expected just from studying uncertainty in for instance mean seasonal temperature or precipitation changes. More precisely, the projection of particularly strong increases in heat stress in central Europe in L13 appears to be more uncertain than the projection of moderate increases of heat stress in

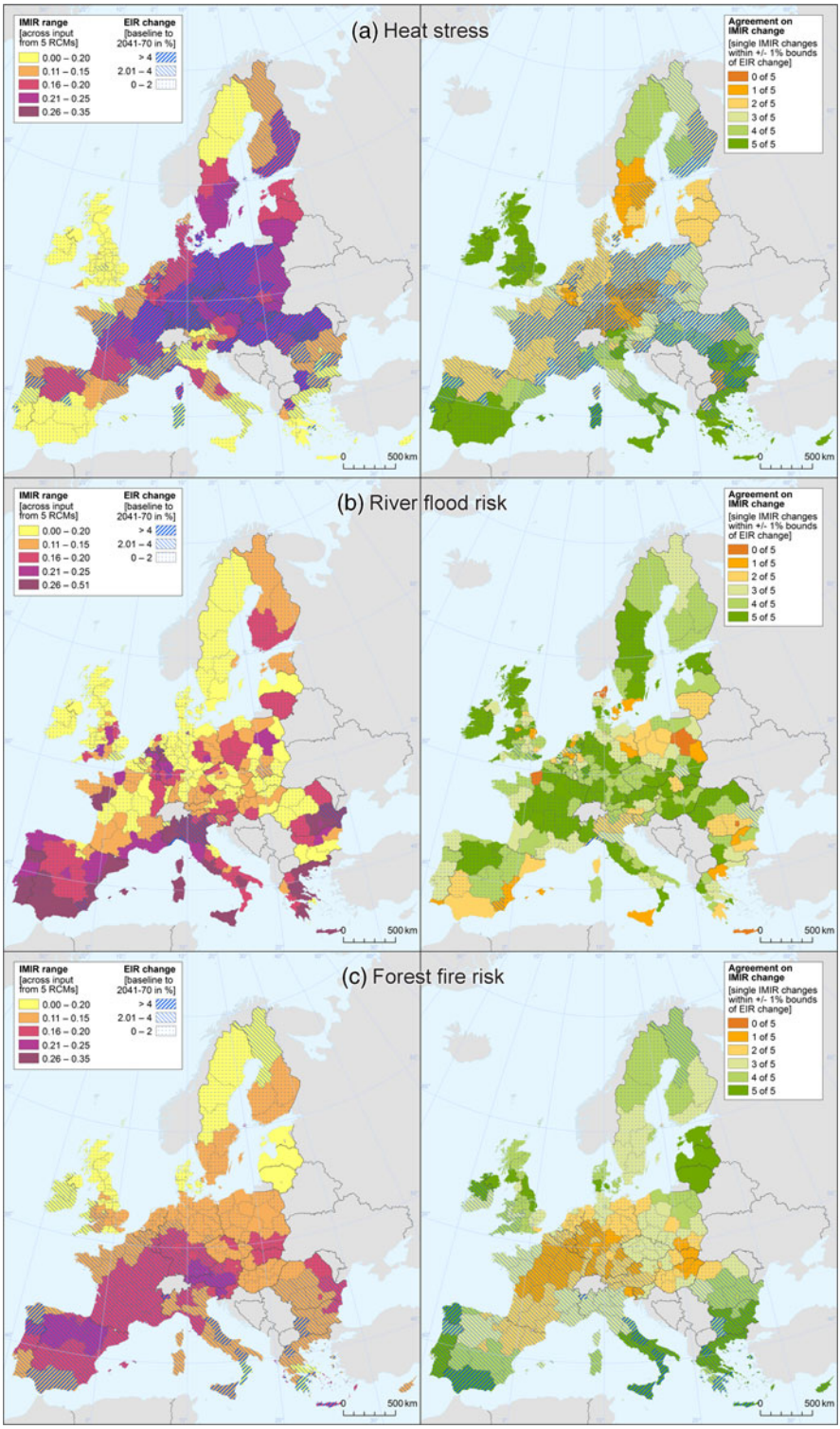
(a) Heat stress
IMIR range
[across input from 5 RCMs]
0.00 – 0.20
0.11 – 0.15
0.16 – 0.20
0.21 – 0.25
0.26 – 0.35
EIR change
[baseline to 2041-70 in %]
> 4
2.01 – 4
0 – 2
Agreement on IMIR change
[single IMIR changes within +/- 1% bounds of EIR change]
0 of 5
1 of 5
2 of 5
3 of 5
4 of 5
5 of 5
0
500 km
(b) River flood risk
IMIR range
[across input from 5 RCMs]
0.00 – 0.20
0.11 – 0.15
0.16 – 0.20
0.21 – 0.25
0.26 – 0.51
EIR change
[baseline to 2041-70 in %]
> 4
2.01 – 4
0 – 2
Agreement on IMIR change
[single IMIR changes within +/- 1% bounds of EIR change]
0 of 5
1 of 5
2 of 5
3 of 5
4 of 5
5 of 5
0
500 km
(c) Forest fire risk
IMIR range
[across input from 5 RCMs]
0.00 – 0.20
0.11 – 0.15
0.16 – 0.20
0.21 – 0.25
0.26 – 0.35
EIR change
[baseline to 2041-70 in %]
> 4
2.01 – 4
0 – 2
Agreement on IMIR change
[single IMIR changes within +/- 1% bounds of EIR change]
0 of 5
1 of 5
2 of 5
3 of 5
4 of 5
5 of 5
0
500 km

southern Europe. Likewise, the projection of a northwards expansion of high forest fire risk into central Europe in L13 seems to be more uncertain than the strong increases in forest fire risk projected for most southern European regions. For river flood risk, uncertainties due to climate model spread appear to be particularly high in the Mediterranean, as previously reported for Spain and Greece by Kundzewicz et al. (2010). These spatial variations in uncertainty across Europe are perhaps the most interesting result from this study in the context of European policy making.

Uncertainties in future climate change impacts refer particularly to extreme events (e.g. Kundzewicz et al. 2010), a principle to be considered when interpreting the results of this study. The revealed IMIR spread is not a consequence of the spread across the five ENSEMBLES models per se, but is also impacted by the choice of the single input indicators used to the construct the composite indicators of L13. T2MAX25 and T2MIN20 as part of the heat stress indicator, as well as CDDMAX used for the forest fire risk indicator, represent some form of climate extreme defined by a threshold in temperature or precipitation (cf. ECA&D, van Engelen et al. 2008). Such threshold-based indicators tend to show a larger spread across different climate models and also reveal larger variances across Europe, compared to indicators that take into account all values for a given period (e.g. T2MEANsu, PRECsu), as shown in the sensitivity analysis (cf. Section 3.1). Thus, different climate input indicators might potentially lead to results different to those of this study, even if the same five ENSEMBLES GCM/RCM were used. This highlights the importance of a careful input indicator selection, which accounts for the varied aspects of climate exposure but at the same time avoids indicators inappropriate to serve as proxies for a certain hazard.

The assessment of river flood risk, based on 100-year recurrence interval floods as derived from the hydrological model LISFLOOD, revealed the generally largest spread across the five IMIRs (cf. Fig. 2a). This is not surprising, as flood risk (a) hinges heavily on rainfall (that is more difficult to simulate than temperature), (b) is linked to hydrological differences that are inherently difficult to detect, and (c) is associated with numerous sources of uncertainty other than those coming from the climate signal (Wilby et al. 2008). In particular, additional uncertainties are introduced due to river flow routing, the process of deriving and defining events with a 100-year return period, and the planar approximation approach to convert river discharge into flood extent and water depth (Feyen et al. 2012).

This study certainly has a number of constraints. The number of GCMs and RCMs is limited, and ideally all GCM/RCM combinations available from the ENSEMBLES project could have been considered. In addition, the analysis considers only a single emission scenario, i.e. SRES A1B. However, since the different SRES scenarios start diverging strongly only towards the end of the century (cf. Nakićenović and Swart 2000), for this mid-century (2041–2070) analysis, most of the variations due to emission scenario are likely to be within the variability due to climate model choice. Another constraint is the focus on the influence of the climatic input to the hazard-specific composite indicators of L13; while uncertainties related to non-climatic inputs (e.g. land use data, demographic data) were not taken into consideration. In that context it should be stressed that the sensitivity analysis investigates the spatial variance in the indicators. It is not an analysis of uncertainty, and therefore does not show, how uncertainty from non-climatic inputs compares with climatic ones. Such an analyses would only be possible if multiple realisations of the non-climatic inputs had been available or at least if their probability distribution could be estimated reliably. Also, the influence of the impact model, in our case the methodological choices to construct the composite indicators of L13, such as data normalisation and aggregation (OECD 2008), have were evaluated here. This could be a direction of future work.

However, previous research has concluded that the (non-) acceptance of climate impact assessment results among decision makers might be particularly associated with scepticism towards the climate information (e.g. Rannow et al. 2010). In that sense, this study may help to gain a better idea of (un)certainty patterns across European regions inherent to the composite impact indicators by L13. Given the fact that indicators are considered to play an ever increasing role in EU policy making (White and Zwirner 2007) this seems to be of particular importance. From a decision-makers' perspective, for regions with low model agreement the results call for an in-depth analysis based on additional models to derive more conclusive patterns. Ultimately, prioritising adaptation options and eventually implementing adaptation actions at the local scale will also require additional information on location-specific sources of uncertainty. For regions where different models have a similar climate signal, such as for heat stress and forest fire risk in southern Europe, the results might help to gain further confidence in the projected impacts, and thus help prioritising action at the EU level with respect to adaptation planning, coordination, and financing.

Acknowledgements This work was funded by the Research Directorate-General of the European Commission through its Seventh Framework Programme project RESPONSES (Grant Agreement number 244092). We thank four anonymous reviewers for their constructive comments.

Disclaimer The views expressed are purely those of the authors and may not in any circumstances be regarded as stating an official position of the European Commission.

References

Ahmad QK, Warrick RA, Downing TE, Nishioka S, Parikh KS, Parmesan C, Schneider SH, Toth F, Yohe G (2001) Methods and tools. In: McCarthy JJ, Canziani OF, Leary NA, Dokken DJ, White KS (eds) Climate change 2001: impacts, adaptation, and vulnerability. Contribution of working group II to the third assessment report of the intergovernmental panel on climate change. Cambridge University Press, Cambridge, pp 105–143

Alcamo J, Moreno JM, Nováky B, Bindi M, Corobov R, Devoy RJN, Giannakopoulos C, Martin E, Olesen JE, Shvidenko A (2007) Europe. In: Parry ML, Canziani OF, Palutikof JP, van der Linden PJ, Hanson CE (eds) Climate change 2007: impacts, adaptation and vulnerability. Contribution of working group II to the fourth assessment report of the intergovernmental panel on climate change. Cambridge University Press, Cambridge, pp 541–580

Botev ZI, Grotowski JF, Kroese DP (2010) Kernel density estimation via diffusion. Ann Stat 38:2916–2957

Carvalho AC, Carvalho A, Martins H, Marques C, Rocha A, Borrego C, Viegas DX, Miranda AI (2010) Fire weather risk assessment under climate change using a dynamical downscaling approach. Environ Modell Softw 26:1123–1133

Christensen JH, Carter TR, Giorgi F (2002) PRUDENCE employs new methods to assess European climate change. Eos 83:147

Christensen JH, Kjellström E, Giorgi F, Lenderink G, Rummukainen M (2010) Weight assignment in regional climate models. Climate Res 44:179–194

Dankers R, Feyen L (2009) Flood hazard in Europe in an ensemble of regional climate scenarios. J Geophys Res 114:D16108

Donat MG, Leckebusch GC, Wild S, Ulbrich U (2011) Future changes in European winter storm losses and extreme wind speeds inferred from GCM and RCM multi-model simulations. Nat Hazard Earth Syst Sci 11:1351–1370

Dosio A, Paruolo P (2011) Bias correction of the ENSEMBLES high resolution climate change projections for use by impact models: evaluation on the present climate. J Geophys Res 116:D16106

Dosio A, Paruolo P, Rojas R (2012) Bias correction of the ENSEMBLES high resolution climate change projections for use by impact models: analysis of the climate change signal. J Geophys Res 117:D17110

EEA-JRC-WHO (2008) Impacts of Europe's changing climate – 2008 indicator-based assessment. Joint EEA-JRC-WHO report, EEA Report No 4/2008, JRC Reference Report No JRC47756. EEA, Copenhagen

ESPON (2011) Climate change and territorial effects on regions and local economies. ESPON climate project, final report, version 31/5/2011. TU Dortmund University, Germany

Feyen L, Dankers R, Bódis K, Salamon P, Barredo JI (2012) Fluvial flood risk in Europe in present and future climates. Clim Change 112:47–62

Füssel HM, Klein RJT (2006) Climate change vulnerability assessments: an evolution of conceptual thinking. Clim Change 75:301–329

Hagemann S, Chen C, Haerter OJ, Heinke J, Gerten D, Piani C (2011) Impact of a statistical bias correction on the projected hydrological changes obtained from three GCMs and two hydrology models. J Hydrometeorol 12:556–578

Hinkel J, Nicholls RJ, Vafeidis AT, Tol RSJ (2010) Assessing risk of an adaptation to sea-level rise in the European Union: an application of DIVA. Mitig Adapt Strateg Glob Change 15:703–719

IPCC (2007) Summary for Policymakers. In: Solomon S, Qin D, Manning M, Chen Z, Marquis M, Averyt KB, Tignor M, Miller HL (eds) Climate change 2007: the physical science basis. Contribution of working group I to the fourth assessment report of the intergovernmental panel on climate change. Cambridge University Press, Cambridge, pp 1–18

Jansen MJW (1999) Analysis of variance designs for model output. Comput Phys Commun 117:35–43

Kundzewicz ZW, Lugeri N, Dankers R, Hirabayashi Y, Döll P, Pińskwar I, Dysarz T, Hochrainer S, Matczak P (2010) Assessing river flood risk and adaptation in Europe – review of projections for the future. Mitig Adapt Strateg Glob Change 15:641–656

Lissner TK, Holsten A, Walther C, Kropp JP (2012) Towards sectoral and standardised vulnerability assessments: the example of heatwave impacts on human health. Clim Change 112:687–708

Lopez A, Fung F, New M, Watts G, Weston A, Wilby RL (2009) From climate model ensembles to climate change impacts and adaptation: a case study of water resource management in the southwest of England. Water Resour Res 45:W08419

Lung T, Lavalle C, Hiederer R, Dosio A, Bouwer LM (2013) A multi-hazard regional level impact assessment for Europe combining indicators of climatic and non-climatic change. Global Environ Change 23:522–536

Maslin M, Austin P (2012) Climate models at their limit? Nature 486:183–184

Nakićenović N, Swart R (eds) (2000) Emissions scenarios 2000. Special report of the intergovernmental panel on climate change. Cambridge University Press, Cambridge

OECD (2008) Handbook on constructing composite indicators: methodology and user guide. OECD Publishing

Olsson J, Yang W, Graham LP, Rosberg J, Andreasson J (2011) Using an ensemble of climate projections for simulating recent and near-future hydrological change to lake Vänern in Sweden. Tellus 63A:126–137

Piani C, Haerter JO, Coppola E (2010) Statistical bias correction for daily precipitation in regional climate models over Europe. Theor Appl Climatol 99:187–192

Rannow S, Loibl W, Greiving S, Gruehn D, Meyer BC (2010) Potential impacts of climate change in Germany – identifying regional priorities for adaptation activities in spatial planning. Landscape Urban Plan 98:160–171

Rojas R, Feyen L, Bianchi A, Dosio A (2012) Assessment of future flood hazard in Europe using a large ensemble of bias corrected regional climate simulations. J Geophys Res 117:D17109

Rosenzweig C, Wilbanks TJ (2010) The state of climate change vulnerability, impacts, and adaptation research: strengthening knowledge base and community. Clim Change 100:103–106

Saltelli A, Ratto M, Andres T, Campolongo F, Cariboni J, Gatelli D, Saisana M, Tarantola S (2008) Global sensitivity analysis: the primer. John Wiley & Sons, Chichester

Saltelli A, Annoni P, Azzini I, Campolongo F, Ratto M, Tarantola S (2010) Variance based sensitivity analysis of model output. Design and estimator for the total sensitivity index. Comput Phys Commun 181:259–270

Sobol' IM (1993) Sensitivity estimates for nonlinear mathematical models. Math Model Comput Exp 1:407–414

Teutschbein C, Seibert J (2010) Regional climate models for hydrological impact studies at the catchment scale: a review of recent modeling strategies. Geogr Compass 4:834–860

van der Knijff J, Younis J, De Roo A (2010) LISFLOOD: a GIS-based distributed model for river basin scale water balance and flood simulation. Int J Geogr Inf Sci 24:189–212

van der Linden P, Mitchell JFB (2009) ENSEMBLES: climate change and its impacts – summary of research and results from the ENSEMBLES project. Met Office Hadley Centre, Exeter

van Engelen A, Klein Tank A, van der Schrier G, Klok L (2008) European Climate Assessment & Dataset (ECA&D), Report 2008, "Towards an operational system for assessing observed changes in climate extremes". KNMI, De Bilt, The Netherlands, 68pp

White S, Zwirner O (2007) The use of indicators in the European Commission. Background paper for beyond GDP conference. European Commission, DG Environment, Brussels

Wilby RL, Beven KJ, Reynard NS (2008) Climate change and fluvial risk in the UK: more of the same? Hydrol Process 22:2511–2523